Available online at www.sciencedirect.com
SCIENCE DIRECT®
Journal of Solid State Chemistry 178 (2005) 3405–3413
JOURNAL OF SOLID STATE CHEMISTRY
www.elsevier.com/locate/jssc

Exploring the distribution of copper–Schiff base complex covalently anchored onto the surface of mesoporous MCM 41 silica

Udayshankar G. Singh[a,1], Ruth T. Williams[a,*], Keith R. Hallam[b], Geoffrey C. Allen[b]

[a]*Department of Chemistry, The Open University, Milton Keynes MK7 6AA, UK*
[b]*Interface Analysis Centre, University of Bristol, Bristol BS2 8BS, UK*

Received 7 July 2005; received in revised form 27 August 2005; accepted 28 August 2005
Available online 29 September 2005

Abstract

A series of copper–Schiff base MCM 41 materials, synthesized by post-synthetic grafting, was studied by X-ray photoelectron spectroscopy (XPS) and nitrogen sorption (77 K) to explore distribution of the copper–Schiff base complex immobilized on the porous Si-MCM 41. Additional information on the physico-chemical properties of the functionalized materials was obtained by powder X-ray diffraction (XRD), atomic absorption spectroscopy (AAS), CHN microanalysis, FTIR spectroscopy, ^{29}Si and ^{13}C CP MAS NMR spectroscopy. The effect of copper–Schiff base complex loading and reaction times on the surface properties of Si-MCM 41 (surface area and pore parameters) in addition to its distribution within the Si-MCM 41 was explored by nitrogen sorption and XPS coupled with argon etching. Argon etching of a surface to a depth of 45 Å confirmed that the copper–Schiff base complex was distributed both on the external surface (pore end) and within the pores of Si-MCM 41. The amount of complex located in the pores at this depth was about one-third of the amount detected on the external surface of MCM 41. Nitrogen sorption isotherms measured at 77 K confirmed the reduction in total pore volume and surface area was the result of pore narrowing of Si-MCM 41 following grafting of complex in the 8 h samples. A significant decrease in surface area and pore volume for the 20 h sample (longer reaction time), with the highest copper loading (0.65 mmol g^{-1}), confirmed pore blocking in this material. The uneven distribution of the copper complex between the external and internal surface of Si-MCM 41 was attributed to the bulky nature of the complex, which restricted access to the pores.

Keywords: Si-MCM 41 support; Copper–Schiff base complex; Nitrogen sorption; X-ray photoelectron spectroscopy; Argon etching

1. Introduction

A general strategy for converting a homogeneous process into a heterogeneous one is to anchor the soluble catalyst onto large surface area inorganic supports [1,2]. The main advantages of heterogenization are the easy separation of the catalyst from the reaction mixture, allowing the possibility to recover and reuse the catalyst, and the possibility of continuous-flow operation. The common problem of this methodology is leaching of the active sites from the solid surface into the solutions, when applied to liquid-phase reactions. However, this can be avoided or minimized by covalently anchoring the active sites onto the inorganic solid supports [3]. As a support, MCM 41 silicas [4] have been widely used since the performance of this material in catalysis is directly related to a structure possessing hexagonally packed arrays of one-dimensional cylindrical pores, with pore diameters ranging between 20 and 100 Å, large surface areas of up to 1500 m^2 g^{-1} and pore volumes up to 1.3 cm^3 g^{-1} [5]. These properties of the MCM 41 support ensure easy accessibility of reactants to the active sites, and functionalization of bulky catalytic sites within the pores. Aside from all these advantages, the most significant disadvantage of the siliceous MCM 41 is that the material is catalytically

*Corresponding author. The Open University in the South West, 4, Portwall Lane, Bristol BS1 6ND, UK. Fax: +44 117 925 5215.
E-mail addresses: usingh@engr.ucsb.edu (U.G. Singh), r.t.williams@open.ac.uk (R.T. Williams), k.r.hallam@bristol.ac.uk (K.R. Hallam), g.c.allen@bristol.ac.uk (G.C. Allen).
[1]Department of Chemical Engineering, University of California–Santa Barbara, 10 Mesa Road, Santa Barbara, California 93106, USA.

0022-4596/$ - see front matter © 2005 Elsevier Inc. All rights reserved.
doi:10.1016/j.jssc.2005.08.023

inactive [6]. In the past few years, much effort has been devoted to enhance the catalytic properties of MCM 41 material [6]. Covalent functionalization of the internal surface of an MCM 41 host can be achieved either by post-synthetic grafting of various metal complexes onto the channel walls [6–8] or by incorporating functionalities directly during the preparation [9,10]. Hybrid organic–inorganic materials developed by covalent modification can be more robust than simpler metal oxide-supported materials, and can show catalytic activities similar to their homogeneous analogues [11]. Significant features of this type of catalyst include high selectivity and ability of the catalyst to retain the metal ion even under harsh reaction conditions [6,11].

Copper-containing molecular sieves are important catalysts in many liquid-phase oxidation reactions; for example in epoxidation of alkenes [12], catechol oxidation [13], partial oxidation of alkyl aromatics [14]. The demand for the use of environmentally friendly copper-containing catalyst in the liquid-phase oxidation catalysis provides a powerful means for the development of recyclable catalysts. A number of recent publications have dealt with the immobilization of copper complexes onto inorganic supports, for example, Ghadiri et al. [12] reported the post-synthetic grafting of copper complexes (with bipyridine and macrocycle) between silicate layers of montmorillonite and MCM 41. More recently, Saha et al. [15] encapsulated copper–Schiff base complex within the pores of Y-zeolite, which showed excellent activity towards hydroxylation of phenol and 1-naphthol. Karandikar et al. [16] reported the immobilization of copper–Schiff base complex onto the $-NH_2$ modified MCM 41, which showed higher activity in the epoxidation of styrene, cyclohexene and 1-decene.

Our preliminary studies (not reported in the paper) involving post-synthetic binding of Cu^{2+} on the Schiff base grafted Si-MCM 41 yielded predominantly direct binding of the copper on the MCM 41 surface, together with 1:1 copper:Schiff base complex rather than the expected 1:2 copper:Schiff base complex. To avoid the direct immobilization of Cu^{2+} on the Si-MCM 41 surface, we have synthesized copper–Schiff base complex first and then carried out the post-synthetic grafting of the complex on the Si-MCM 41 support. In this paper, we report the synthesis of copper–Schiff base MCM 41 materials covalently anchored onto the Si-MCM 41 surface by the esterification of siloxane groups and surface silanol groups of Si-MCM 41. A series of copper–Schiff base MCM 41 materials was synthesized to study the effect of copper loadings and reaction times on the surface properties of the material. A detailed characterization of the functionalized material was obtained by powder X-ray diffraction (XRD), atomic absorption spectroscopy (AAS), CHN microanalysis, infrared spectroscopy, ^{29}Si and ^{13}C CP (cross-polarized) MAS NMR spectroscopy, nitrogen sorption at 77 K and X-ray photoelectron spectroscopy (XPS) coupled with argon etching.

2. Experimental

2.1. Synthesis of the Si-MCM 41 material

Tetraethyl orthosilicate 98% (TEOS, Aldrich), a 25% by mass aqueous solution of cetyltrimethylammonium chloride (CTMACl, Aldrich), 3-aminopropyl triethoxysilane 97% (Aldrich), salicylaldehyde 99% (Aldrich), copper (II) acetate anhydrous (Alfa Aesar) were used as received.

The parent siliceous MCM 41 material was synthesized by hydrolysis of TEOS under mild alkali conditions. The synthetic procedure for Si-MCM 41 has been previously described elsewhere [17].

2.2. General method for the synthesis of copper–Schiff base MCM 41 material

Scheme 1 shows the general method we have used for the synthesis of copper–Schiff base MCM 41 material. Here, the structure of the product **I** is shown generalized as having two Si–O bonds to the surface; however, the precise value may vary depending on the local surface coverage of silanol groups.

The grafting of copper–Schiff base was carried out in two steps: First, the Schiff base ligand was prepared by reacting aminopropyl triethoxysilane with salisylaldehyde [18,19]. The detailed procedure was as follows: aminopropyl triethoxysilane (2.32 mmol) was added to salisylaldeyhde (2.34 mmol) in methanol (50 cm^3) and the resultant mixture was refluxed for 3 h. The solvent was removed by evaporation from the yellow viscous Schiff base triethoxysilane ligand, which had been formed in a 1:1 molar ratio. The complex formed was analyzed using infrared spectroscopy for the presence of the imine group.

Second, copper–Schiff base MCM 41 materials were prepared by refluxing in toluene (40 cm^3) for 3h, appropriate amounts of the Schiff base triethoxysilane ligand (0.49, 1.01, 1.53 or 2.30 mmol) and the copper acetate (0.32, 0.63, 0.95 or 1.26 mmol) in a 2:1 molar ratio. Template-free Si-MCM 41 (1.00 g, preheated at 100 °C for 2 h) was then added and was further refluxed for 5 or 17 h. The resulting yellowish green solid formed was collected by filtration under air, washed with ethanol (2×25 cm^3) and acetone (2×10 cm^3), and then dried in vacuo (2 h) and then in an oven at 50 °C for 12 h to give final product **I**, Scheme 1. The details of the reaction times and the amount of precursors used in the synthesis of the copper–Schiff base MCM 41 materials are given in Table 1.

2.3. Instrumentation

The hexagonal structures of the parent and copper–Schiff base modified MCM 41 materials were measured with a Philips PW 1050/81 diffractometer operating in Bragg–Brentano geometry with CrK_α radiation ($\lambda = 2.290$ Å) and equipped with a diffracted beam monochromator. Data were collected in the 2θ range 1–10° with

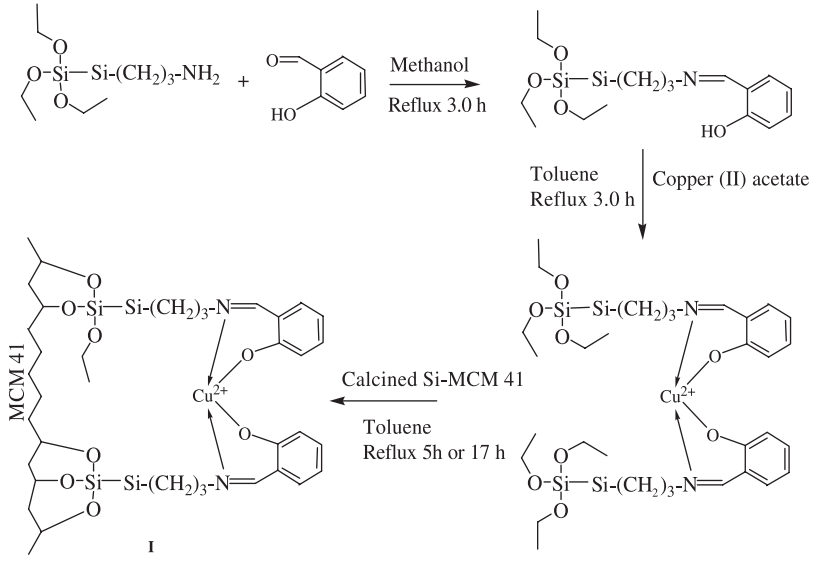

Scheme 1. Synthesis of covalently functionalized copper–Schiff base MCM 41.

Table 1
Summary of CHN and AAS data for the functionalized copper–Schiff base MCM 41 samples

Sample	Total reaction time (h)	Schiff base triethoxysilane (mmol g^{-1})	Nominal loading of copper (mmol g^{-1})	Copper analysis (AAS) (mmol g^{-1})	Analysis C, H, N, (%)	Nitrogen/ copper mol ratio
Si-MCM 41	—	—	—	—	0.08, 1.10, 0.00	—
Cu–Schiff–MCM-**0.25**(8)	8	0.49	0.25	0.25	7.16, 1.67, 0.59	1.7
Cu–Schiff–MCM-**0.50**(8)	8	1.01	0.50	0.35	9.42, 2.01, 0.86	1.8
Cu–Schiff–MCM-**0.75**(8)	8	1.53	0.75	0.45	10.96, 2.20, 1.11	1.8
Cu–Schiff–MCM-**1.0**(8)	8	2.30	1.05	0.47	11.46, 2.24, 1.16	1.8
Cu–Schiff–MCM-**1.0**(20)	20	2.30	1.05	0.65	14.59, 1.96, 1.65	1.8

a step size of 0.05° and dwell time of 5 s per point. Analysis for copper was performed using AAS using a Perkin-Elmer Analyst 100 spectrometer. An air/acetylene fuel in a ratio of 3:1 litres per minute was used for analysis. Samples (ca. 0.100 g) were dissolved in 1:1 mixture of HF/HNO_3 (5 cm^3) prior to analysis. Elemental analysis, for carbon hydrogen and nitrogen (CHN), was performed using a Carlo Erba 1110 CHN Elemental Analyser. Samples masses of 10 mg rather than the usual 2 mg were used for greater precision. FTIR spectra were recorded for samples after being pressed into 13 mm discs with freshly dried KBr salt. Spectra were recorded at room temperature with a Nicolet 550 Magna IR spectrometer at a resolution of 4 cm^{-1}, with 32 scans per sample. Both ^{29}Si and ^{13}C MAS NMR spectra were recorded on a Bruker MS-300 spectrometer operating at Larmor frequency of 59.62 and 75.46 MHz, respectively. To enhance the sensitivity cross-polarization (CP) technique was employed. Nitrogen isotherms were measured at 77 K using an automated sorption equipment, the Micromeritics Tristar 3000. Data were collected on a PC and calculations of surface and pore properties were subsequently performed using the Micromeritics software, TriStar 3000 v2.00. Prior to measurement, the parent Si-MCM 41 was purged with flowing nitrogen gas at 150 °C for 6 h and the functionalized materials were purged at 100 °C for 6 h. The low temperature was used to avoid any possible decomposition of the functionalized materials. Free space in the sample tube was determined with He, assumed not to adsorb, for each sample. The surface area and pore size distribution were obtained by the BET and BJH methods. X-ray photoelectron spectra were recorded using a Thermo VG Scientific (East Grinstead, England) Escascope using an Mg$K\alpha$ X-ray source operating at 300 W (15 kV; 20 mA). Samples were mounted on a stainless-steel sample holder, using double-sided adhesive carbon tabs. The wide binding energy range survey spectra were obtained using an analyser pass energy of 50 eV, whereas high-resolution spectra of selected elements were taken at 30 eV pass energy. The C 1*s* peak from adventitious hydrocarbon, expected at 284.8 eV binding energy, was used to correct the binding energy for sample charging effects [20]. Quantification and peak-fitting of the data were performed using the VGS5250 software supplied with the spectrometer, based on the use of linear backgrounds beneath the peaks of interest and the quantification relative sensitivity factors supplied by the manufacturer.

3. Results and discussion

The series of copper–Schiff base MCM 41 materials synthesized by post-synthetic grafting of Si-MCM 41 with an 8 h reaction time includes four samples with nominal copper loadings in the range 0.25–1.0 mmol g^{-1} and are denoted as Cu–Schiff–MCM-**0.25(8),** Cu–Schiff–MCM-**0.50(8)**, Cu–Schiff–MCM-**0.75(8)** and Cu–Schiff–MCM-**1.0(8)**, and a 20 h reaction time sample with a nominal copper loading of 1.0 mmol g^{-1} as Cu–Schiff–MCM-**1.0(20)**.

The powder XRD patterns for the parent Si-MCM 41 and samples derived by post-synthetic grafting of the copper–Schiff base complex are shown in Fig. 1. The powder XRD pattern of the parent Si-MCM 41 sample shows three low-angle reflections (d_{100}, d_{110}, d_{200}) characteristic of a well-ordered hexagonal pore arrangement and a d_{100} spacing value of 37 Å [21]. All copper–Schiff base MCM 41 samples exhibited only one d_{100} reflection with a d_{100} spacing of 37 Å except for the Cu–Schiff–MCM-**1.0(20)** sample, which showed a d_{100} spacing of 36 Å. After the post-synthetic grafting, the position of d_{100} reflection remained virtually constant in all the samples, suggesting that the hexagonal pore arrangement of Si-MCM 41 is intact. However, upon post-synthetic grafting the d_{110} and d_{200} reflections were no longer observed, and an overall decrease in the intensity of d_{100} was observed. This decrease in intensity was significant for the Cu–Schiff–MCM-**1.0(20)** sample. These results could be attributed to lower local order, such as variations in the wall thickness or as it was previously mentioned by Lim et al. [22], this is due to contrast matching between the amorphous silicate framework and copper–Schiff base complex that are located inside the channels of Si-MCM 41.

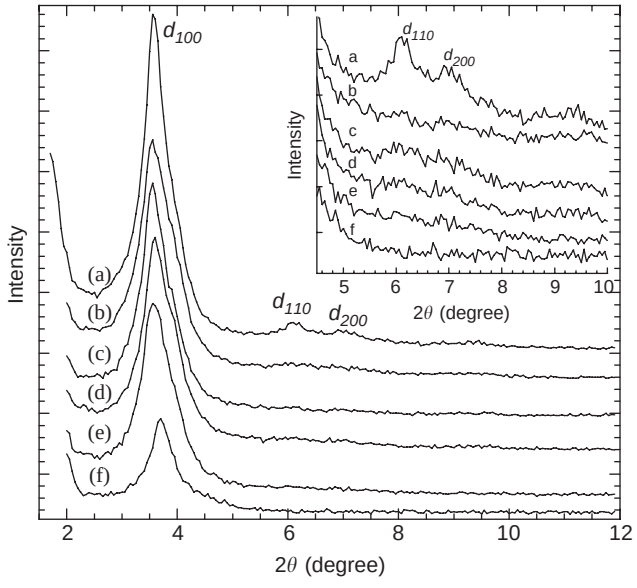

Fig. 1. Powder XRD patterns of: (a) parent Si-MCM 41; (b) Cu–Schiff–MCM-**0.25**(8); (c) Cu–Schiff–MCM-**0.50**(8); (d) Cu–Schiff–MCM-**0.75**(8); (e) Cu–Schiff–MCM-**1.0**(8); (f) Cu–Schiff–MCM-**1.0**(20).

The copper loading determined by AAS are summarized in Table 1. The data show that we succeeded in immobilizing virtually all of the copper–Schiff base complex onto the Si-MCM 41 support at the lower copper loading of 0.25 mmol g^{-1}, i.e. for the Cu–Schiff–MCM-**0.25(8)** sample. The copper loading appears to level-off at a maximum of 0.47 mmol g^{-1} for the 8 h samples, but by using a longer reaction time of 20 h increases the copper loading to 0.65 mmol g^{-1}.

The elemental analysis data in Table 1 show an increase in mass percentage of CHN with increased nominal loading of copper–Schiff base complex and with longer reaction time. This confirms the immobilization of copper–Schiff base complex on Si-MCM 41 support and is consistent with the AAS results. The observed nitrogen/copper molar ratio of 1.8 for all samples is in close agreement with the expected value of 2.0. This confirms that the functionalization of copper onto the Si-MCM 41 support proceeds with the intended copper–Schiff base complex format in a 1:2 (copper/Schiff base) molar ratio.

The FTIR spectra of all copper–Schiff base MCM 41 samples were similar. Fig. 2 shows the FTIR spectrum of the Cu–Schiff–MCM-**0.25(8)** material as a typical example. The spectrum shows all of the principal bands for the Schiff base ligand. The sharp band at 1625 cm^{-1} was assigned to –C═N stretching vibration of the imine group [23]. This band in free ligand (spectrum not shown here) appears at 1642 cm^{-1} and undergoes small shifts to lower frequencies in the spectra of the copper–Schiff base complexes indicating coordination of the imine nitrogen with copper. The bands at 1542 and 760 cm^{-1} were assigned to ν (Ph–)C–C(═N) bond [24] (–C═N– group conjugated with phenyl ring) and an aromatic out-of-plane C–H deformation vibration, respectively. The expected C–H stretching and deformation bands are visible between

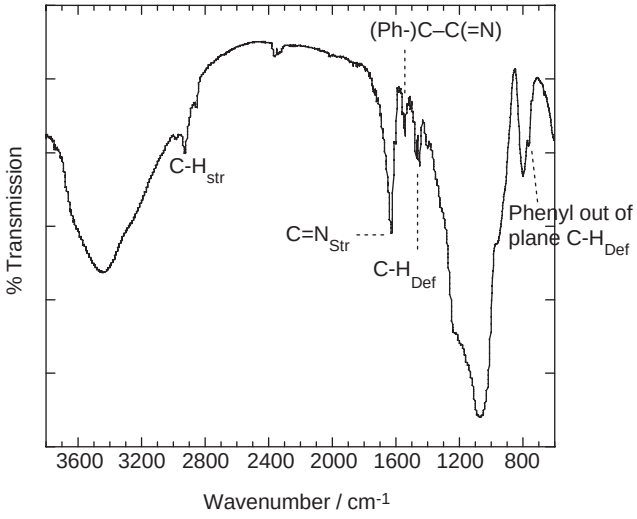

Fig. 2. FTIR spectrum of the Cu–Schiff–MCM-**1.0(8)** sample.

2800–3000 cm^{-1} and 1400–1500 cm^{-1}, respectively. All these bands were also observed in the spectrum of a free copper–Schiff base ligand (spectrum not shown here) but were absent in the spectrum of parent Si-MCM 41, i.e. prior to functionalization. The FTIR result confirms the formation of copper–Schiff base complex and its immobilization within the pores of parent Si-MCM 41, which is consistent with the CHN elemental and AAS results.

Solid state ^{29}Si MAS NMR provides information about the silicon environment and about the degree of functionalization. Fig. 3 shows ^{29}Si CP MAS NMR spectra of the parent Si-MCM 41 sample and the Cu–Schiff–MCM-**0.25(8)** sample as a typical example. The spectrum for the Si-MCM 41 sample shows three distinct resonances at −91.9, −101.8 and −109.3 ppm assigned to Q^2, Q^3 and Q^4, respectively, characteristic of the silica network [$Q^n = Si(OSi)_n(OH)4-n$, $n = 2-4$] [21,22,25]. Upon functionalization all copper–Schiff base MCM 41 showed presence of two different types of silicon, i.e. Q^n and T^m. The T^m peaks observed at −57.9 and −66.0 ppm were assigned to T^2 and T^3, respectively, for the silicon attached to carbon [$T^m = RSi(OSi)_m(OH)_{3-m}$, $m = 1-3$] [21]. As expected, the functionalized samples showed a decrease in the intensity of Q^2 and Q^3 resonances and a concomitant increase in the intensity of Q^4 resonance. This decrease in the intensity of Q^2 and Q^3 resonances indicates that the surface –OH groups are utilized in the post-synthetic grafting process by forming ester bonds with the siloxane groups from complex. The presence of T^m peaks and the increase in the Q^4 resonance for the functionalized samples confirms the immobilization of copper–Schiff base complex onto Si-MCM 41 surface.

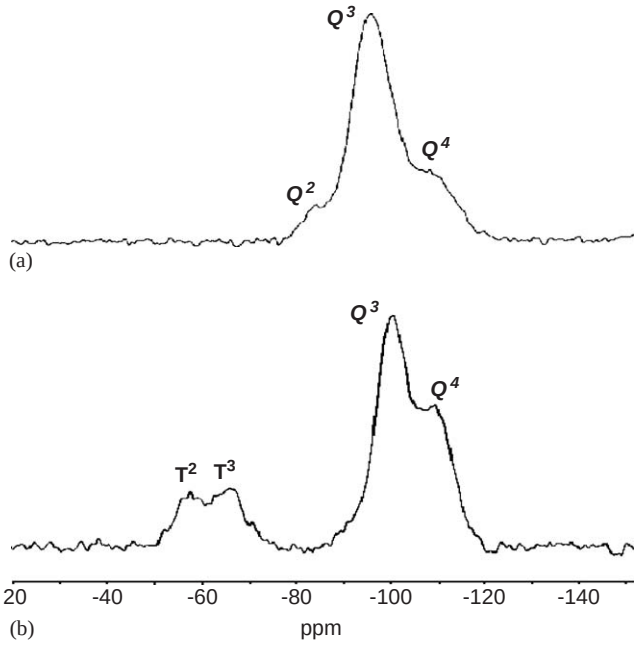

Fig. 3. ^{29}Si CP MAS NMR spectra of: (a) parent Si-MCM 41 sample; (b) Cu–Schiff–MCM-**1.0(8)**.

Fig. 4 shows the ^{13}C CP MAS NMR spectrum of the Cu–Schiff–MCM-**0.25(8)** material as a typical example. The ^{13}C CP MAS NMR spectra of all functionalized samples show peaks corresponding to both the aliphatic and aromatic carbons of the Schiff base. The peaks in the aliphatic region at 10, 24 and 50 ppm were assigned to the three different carbon atoms of the 3-aminopropyl groups [26], which link the metal–Schiff base complex to the MCM 41 surface. The small NMR peak at 60 ppm was assigned to the methylene carbon of the ethoxy groups [26]. The presence of this peak in the NMR spectra suggests all the ethoxy groups are not hydrolysed during post-synthetic grafting. Six peaks from the phenyl ring are expected in the aromatic region; however, the resolution of these peaks in solid state NMR was not achieved under the analysis conditions and the spectrum showed four broad peaks at 119, 134, 162 and 165 ppm [26]. The two peaks at 162 and 165 ppm are due to carbons attached to electronegative atoms. These peaks are assigned to the phenyl carbon atoms attached to the oxygen, (Ph)–O–, and nitrogen, –C═N–CH_2(Ph) in the copper–Schiff base complex.

Nitrogen sorption isotherms for Si-MCM 41 and copper–Schiff base MCM 41 samples are shown in Fig. 5. The parent Si-MCM 41 material showed Type IV isotherm, characteristic of mesoporous materials according to IUPAC classification [27]. The step-wise rise of the adsorbed nitrogen, caused by capillary condensation within the mesopores, was clearly observed in the range $0.20 < P/P^0 < 0.35$. The 8 h series copper–Schiff base MCM 41 samples, i.e. Cu–Schiff–MCM-**0.25(8)** and Cu–Schiff–MCM-**0.50(8)** showed Type IV isotherms, whereas, Cu–Schiff–MCM-**0.75(8)** and Cu–Schiff–MCM-**1.0(8)** samples showed Type IV/I isotherms with an ill-defined capillary condensation region in the range $0.15 < P/P^0 < 0.28$. The 20 h sample, i.e. Cu–Schiff–MCM-**1.0(20)** clearly exhibited a Type I isotherm, characteristic of microporous materials according to IUPAC classification [28]. The progressive change in isotherm from Type IV to Type I with increased copper loading was expected due to the replacement of surface silanol groups by the bulky copper–Schiff base complex. The specific surface areas of all samples were calculated by BET method. The pore sizes and the pore volumes were calculated by BJH and Gurvitsch methods [28], respectively. The BET surface area, pore diameter and pore volume of the parent Si-MCM 41 sample were 1150 $m^2 g^{-1}$, 26 Å and 0.74 $cm^3 g^{-1}$, respectively, typical values for MCM 41 samples prepared under basic conditions. A decrease in surface area and pore volume with increased copper loading was observed, listed in Table 2, which suggests the immobilization of copper–Schiff base complex within the pores of Si-MCM 41. The Cu–Schiff–MCM-**1.0(20)** sample showed a significant decrease in the surface area and pore volume (Table 2) compared with the 8 h sample, which suggests that the increased copper loading achieved by an increase in the reaction time causes blocking of the pore openings.

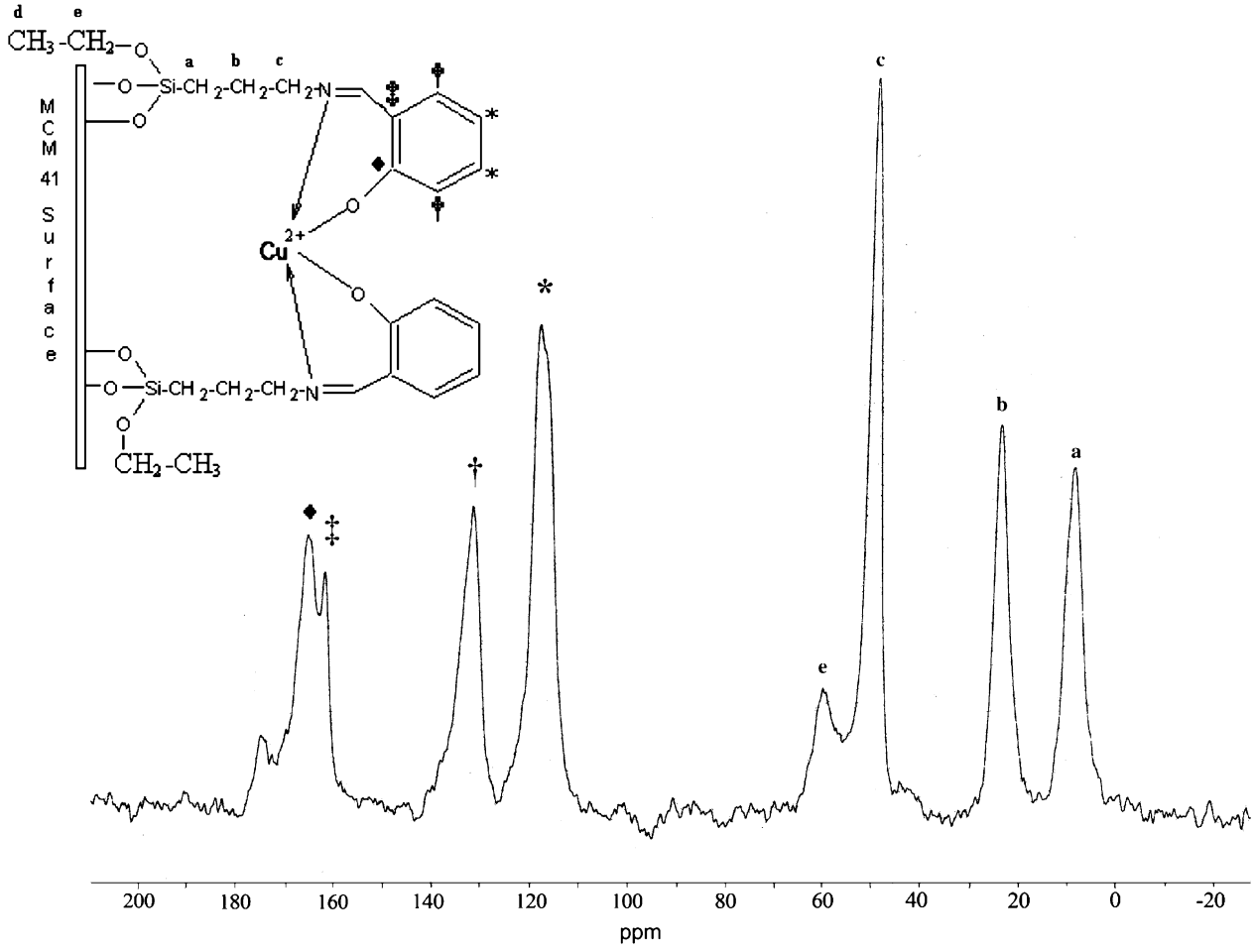

Fig. 4. ^{13}C CP MAS NMR spectrum of the Cu–Schiff–MCM-**1.0(8)** sample.

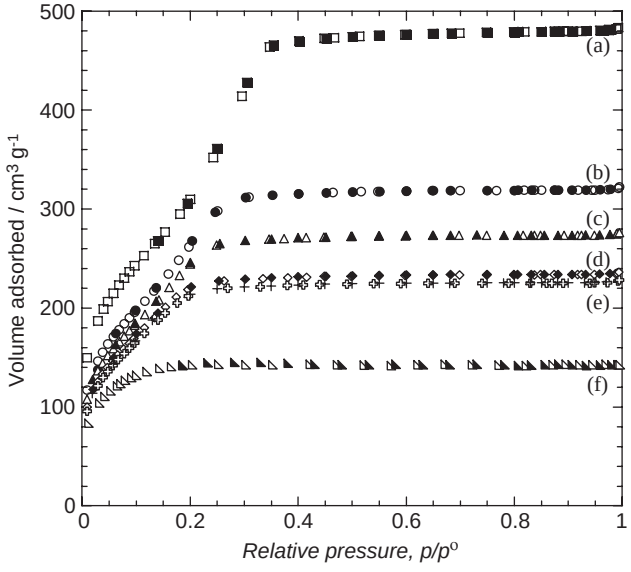

Fig. 5. Nitrogen sorption isotherms at 77 K of: (a) parent Si-MCM 41; (b) Cu–Schiff–MCM-**0.25(8)**; (c) Cu–Schiff–MCM-**0.50(8)**; (d) Cu–Schiff–MCM-**0.75(8)**; (e) Cu–Schiff–MCM-**1.0(8)**; (f) Cu–Schiff–MCM-**1.0(20)**. Filled symbols denote desorption points.

The idea of pore blocking is further supported from predictions of pore volumes from pore width. The pore width for the Cu–Schiff–MCM-**1.0(8)** and the Cu–Schiff–MCM-**1.0(20)** samples was found to decrease by a third, i.e. from 26 to 17 Å and from 26 to 16 Å, respectively, upon functionalization. For cylindrical pores, this should correspond to a predicted decrease in the pore volume from 0.74 to 0.32 $cm^3 g^{-1}$, which is in close agreement with the measured value of 0.34 $cm^3 g^{-1}$ for the Cu–Schiff–MCM-**1.0(8)** sample. However, the Cu–Schiff–MCM-**1.0(20)** sample showed a measured pore volume of 0.20 $cm^3 g^{-1}$. This suggests that a significant pore blocking has occurred for a sample with a reaction time of 20 h compared with the 8 h sample.

XPS is a surface analytical technique, which uses X-rays to excite the emission of photoelectrons from the surface of a sample. The low kinetic energy of the photoelectrons limits the analysis depth of XPS to within the order of 10–50 Å of the upper surface. However, for the analyses presented here, it should be remembered that on the scale of the XPS analysis area, the individual sample grains will

Table 2
Nitrogen sorption results of the Si-MCM 41 and the copper–Schiff base MCM 41 materials

Sample	Isotherm type	S_{BET} ($m^2 g^{-1}$)	V_{pore} ($cm^3 g^{-1}$)	BJH average pore diameter (Å)
Si-MCM 41	IV	1150	0.74	26
Cu–Schiff–MCM-**0.25(8)**	IV	1010	0.49	19
Cu–Schiff–MCM-**0.50(8)**	IV	950	0.42	18
Cu–Schiff–MCM-**0.75(8)**	I/IV	850	0.36	17
Cu–Schiff–MCM-**1.0(8)**	I/IV	825	0.34	17
Cu–Schiff–MCM-**1.0(20)**	I	470	0.20	16

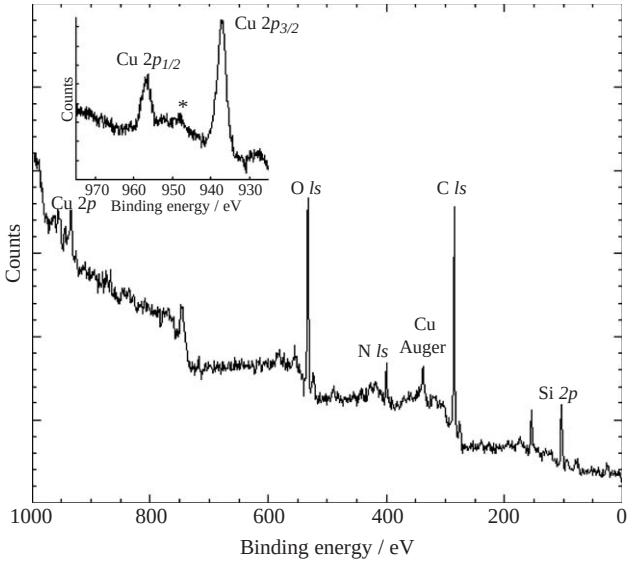

Fig. 6. Wide-scan XPS spectrum of the Cu–Schiff–MCM-**1.0(8)** sample. The inset shows high-resolution spectrum in the Cu 2*p* region (*—Cu satellite peaks).

be randomly oriented. The analyses will be averages of measurements from grains at all orientations, including those presenting the outer faces of the hexagonal structure to the analyser and others end-on, thus contributing information on elements and species within the open ends of the pore structure.

An XPS spectrum of the Cu–Schiff–MCM-**1.0(8)** sample as a typical example is shown in Fig. 6. Table 3 summarizes the measured binding energies, assigned chemical environments and the quantified surface atomic concentrations as determined by XPS.

For the parent Si-MCM 41 sample, the O 1*s* peak position of 533.2 eV is as expected for silica. Likewise, 103.8 eV for the Si 2*p* peak is in agreement with SiO_2-type material. The Si 2*p* peak position for the copper–Schiff base MCM 41 samples was observed at slightly lower binding energy, i.e. at 102.8 eV. The spectra of all functionalized samples as expected showed peaks for N 1*s* at 399.4 eV assigned for imines. The spectra also showed two intense peaks at 935.3 and 955.4 eV assigned to Cu^{2+} $2p_{3/2}$ and $2p_{1/2}$, respectively, along with the Cu satellite peaks [29]. The XPS spectrum in Cu 2*p* region for the Cu–Schiff–MCM-**1.0(8)** sample is shown as inset in Fig. 6. These peaks were absent in the spectrum of Si-MCM 41 and their presence after functionalization confirms the immobilization of copper–Schiff base complex onto Si-MCM 41 surface. No change in the binding energy positions of the elements after argon etching was observed. The spectra showed copper to be present in both the oxidation states, i.e. Cu^{+} and Cu^{2+}. However, careful analysis with short exposure times showed that the presence of two apparent oxidation states is a function of the analysis conditions rather than a fundamental property of the material [18].

The parent Si-MCM 41 and copper–Schiff base MCM 41 samples showed clear differences in the quantified surface atomic concentrations (Table 3), with much increased carbon concentrations present on functionalized samples, nitrogen and copper being present, where they were not prior to functionalization. This is consistent with the CHN microanalysis and AAS results for the immobilization of copper–Schiff base complex. The reduced silicon and oxygen atomic concentration in the copper–Schiff base MCM 41 samples are indicative of Schiff base masking the Si-MCM 41 surface. Argon ion etching for a total of 270 s (at an etch rate of approximately 10 Å per minute, equivalent to ~45 Å depth) brought about a significant increase in the carbon concentration for the parent Si-MCM 41 sample. This is believed to be due to the ion beam redistributing carbon-containing molecules from the adhesive tab used to hold the powder sample. For the functionalized samples, the silicon:copper ratio increased, which could suggest that the copper was predominantly on the surface and preferentially removed by the ion etching. The copper concentration decreases to a third after argon etching, which suggests that one-third of the copper–Schiff base complex was immobilized within the pores and approximately two-thirds is immobilized on the external surface (at the pore end) resulting in some pore blocking. These results are consistent with the nitrogen sorption isotherms, which showed a progressive change in isotherm shape from Type IV to Type I, with increased copper loading. This indicates narrowing and blocking of pores in Si-MCM 41 due to immobilization of copper–Schiff base complex, which results in a decrease in surface area and pore parameter.

Table 3
Summary of the measured binding energies, assigned chemical environments and the quantified surface atomic concentrations as determined by XPS

Sample	Surface atomic concentration/ at%				
	Carbon	Nitrogen	Oxygen	Silicon	Copper
Binding energy (eV)	284.8 (HC)[a] 286.3 (carbon with nitrogen)	399.3 (imines/amines)	531.1 532.9 (SiO_2-Type)	103.1 (silicate)	935.3 (Cu-II) 955.4
Binding energy (eV)[b]	284.8 (HC)[a] 286.2 (carbon with nitrogen)	398.7 (imines/amines)	531.1 532.9 (SiO_2-Type)	100.8 102.8 (silicate)	933.6 (Cu-I) 953.6 935.4 (Cu-II) 955.5
Si-MCM 41	3.3	—	68.5	28.3	—
Si-MCM 41[b]	32.1	—	45.8	22.1	—
Cu–Schiff–MCM-**1.0(8)**	65.0	4.7	21.2	8.2	0.9
Cu–Schiff–MCM-**1.0(8)**[b]	50.6	3.3	28.0	17.8	0.3
Cu–Schiff–MCM-**0.75(8)**	61.8	5.1	22.6	9.5	1.0
Cu–Schiff–MCM-**0.75(8)**[b]	48.9	1.8	30.2	18.8	0.3
Cu–Schiff–MCM-**0.50(8)**	54.1	4.4	28.6	12.0	0.9
Cu–Schiff–MCM-**0.50(8)**[b]	45.1	1.5	32.5	20.6	0.2
Cu–Schiff–MCM-**0.25(8)**	48.3	3.9	33.1	13.8	0.9
Cu–Schiff–MCM-**0.25(8)**[b]	46.5	1.0	32.3	20.0	0.2
Cu–Schiff–MCM-**1.0(20)**	71.0	5.8	16.2	5.6	1.5
Cu–Schiff–MCM-**1.0(20)**[b]	85.7	3.0	6.6	4.1	0.5

[a]HC = adventitious hydrocarbon.
[b]Samples after argon etching for 270 s (at a rate of ca. 10 Å min^{-1}, equivalent to ~45 Å depth).

4. Conclusions

Covalent functionalization of copper–Schiff base complex onto the Si-MCM 41 surface was successfully achieved by post-synthetic grafting. The effect of copper–Schiff base complex loading and reaction times on the physical properties of Si-MCM 41 (surface area and pore parameters) in addition to its distribution within the Si-MCM 41 was explored by nitrogen sorption and XPS coupled with argon etching.

The presence of d_{100} in the XRD pattern confirmed that the hexagonal structure of Si-MCM 41 retains after functionalization. The peak at 1625 cm^{-1} in the FTIR spectrum of the functionalized samples confirmed that the copper complexes with Schiff base ligand. AAS data with CHN microanalysis revealed the immobilization of copper in the form of copper–Schiff base complex onto the Si-MCM 41 surface. Solid state ^{29}Si CP MAS NMR showed that the immobilization of copper–Schiff base complex onto Si-MCM 41 surface took place by esterification of siloxane groups with the surface hydroxyls.

Nitrogen sorption isotherms measured at 77 K showed a progressive change in isotherm from Type IV to Type I with increased copper loading. This confirmed that the immobilization of copper–Schiff base complex causes pore narrowing, which results in decrease in the mesoporosity of Si-MCM 41. This was also supported by a decrease in surface area, pore volume and pore diameter of Si-MCM 41 following functionalization. A significant decrease in surface area and pore volume for the material with the highest copper loading (0.65 mmol g^{-1}) and longer reaction time (20h compared with 8h) confirmed pore blocking in this material. Argon etching of the surface to a depth of 45 Å coupled with XPS confirmed that the copper–Schiff base complex was distributed both onto the external surface and within the pores of Si-MCM 41. However, only a third of the complex was located within the pores and rest onto the end of pore opening or onto the external surface of Si-MCM 41. The uneven distribution of the copper complex between the external and internal surface of Si-MCM 41 was attributed to the bulky nature of the complex, which restricted access to the pores.

Acknowledgments

We thank Robin Hollman (University of Exeter, UK) for CHN microanalysis and Dr. A. Herve (University College London, UK) for NMR analysis. U.G. Singh thanks the Open University for financial support, and the School of Chemistry (University of Exeter, UK) for the use of its facilities.

References

[1] C.A. McNamara, M.J. Dixion, M. Bradely, Chem. Rev. 102 (2002) 3275.
[2] N.E. Leadbeater, M. Marco, Chem. Rev. 102 (2002) 3217.
[3] C. Baleizão, B. Gigante, D. Das, M. Álvaro, H. Garcia, A. Corma, J. Catal. 223 (2004) 106.
[4] C.T. Kresge, M.E. Leonowicz, W.J. Roth, J.C. Vartuli, J.S. Beck, Nature 359 (1992) 710.
[5] S.J. Beck, J.C. Vartuli, W.J. Roth, M.E. Leonowicz, C.T. Kresge, K.D. Schmitt, C.T. Chu, D.H. Olson, E.W. Sheppard, S.B. McCullen, J.B. Higgins, L.J. Schlenker, J. Am. Chem. Soc. 114 (1992) 10834.

[6] P.M. Price, J.H. Clark, D.J. Macquarrie, J. Chem. Soc. Dalton Trans. (2000) 101.
[7] L. Mercier, T.J. Pinnavaia, Adv. Mater. 9 (1997) 500.
[8] S. Xiang, Y. Zhang, Q. Xin, C. Li, J. Chem. Soc. Chem. Commun. 22 (2002) 2696.
[9] K. Moller, T. Bein, R.X. Fischer, Chem. Mater. 11 (1999) 665.
[10] Q.S. Huo, D.I. Margolese, G.D. Stucky, Chem. Mater. 8 (1996) 1147.
[11] J.H. Clark, D.J. Macquarrie, Chem. Soc. Rev. (1996) 303.
[12] M. Ghadiri, F. Farzaneh, M. Gandhi, M. Alizadeh, J. Mol. Catal. A: Chem. 233 (2005) 127.
[13] M. Louloudi, K. Mitopoulou, E. Evaggelou, Y. Deligiannakis, N. Hadjiliadis, J. Mol. Catal. A: Chem. 198 (2003) 231.
[14] C.R. Jacob, S.P. Varkey, P. Ratnasamy, Appl. Catal. A: Gen. 182 (1999) 91.
[15] P.K. Saha, S. Koner, Inorg. Chem. Commun. 7 (2004) 1164.
[16] P. Karandikar, K.C. Dhanya, S. Deshpande, A.J. Chandwadkar, S. Sivasanker, M. Agashe, Catal. Commun. 5 (2004) 69.
[17] U.G. Singh, R.T. Williams, K.R. Hallam, G.C. Allen, Solid State Sci., 2005, in press, doi:10.1016/j.solidstatesciences.2005.05.002.
[18] U. Singh, R.T. Williams, I.D. Salter, K.R. Hallam, G.C. Allen, in: F. Rodriguez-Reinoso, B. McEnaney, J. Roquerol, K. Unger (Eds.), Studies in Surface Science and Catalysis, vol. 144, Elsevier Science, 2002, p. 639.
[19] I.C. Chisem, J. Rafelt, M.T. Shieh, J. Chisem, J.H. Clark, R. Jachhuck, D.J. Macquarrie, C. Ramshaw, K. Schott, Chem. Commun. (1998) 1949.
[20] J.F. Moulder, W.F. Stickle, P.E. Sobol, K.D. Bomben, in: J. Chastain (Ed.), Handbook of X-ray Photoelectron Spectra—A Reference Book of Standard Spectra for Identification and Interpretation of XPS Data, Perkin-Elmer Corporation, Eden Prairie, Minnesota, United States of America, 1992.
[21] C. Lesaint, B. Lebeau, C. Marichal, J. Patarin, Microporous Mesoporous Mater. 83 (2005) 76.
[22] M.H. Lim, A. Stein, Chem. Mater. 11 (1999) 3285.
[23] J. Losada, I. del Peso, L. Beyer, Inorg. Chim. Acta 321 (2001) 107.
[24] Wen-Long Liu, Y. Zou, Chun-Lin Ni, Yi-Zhi Li, Q. Meng, J. Mol. Struct. 751 (2005) 1.
[25] C.E. Fowler, S. Mann, B. Lebeau, J. Chem. Soc. Chem. Commun. 17 (1998) 1825.
[26] H. Juvaste, E.I. Iiskola, T.T. Pakkanen, J. Mol. Catal. A: Chem. 1 (1999) 150.
[27] D.H. Everett, Pure Appl. Chem. 31 (1972) 578.
[28] S.J. Gregg, K.W. Sing, Adsorption Surface Area and Porosity, second ed., Academic Press, London, 1982.
[29] Y. Yuan, W. Cao, W. Weng, J. Catal. 228 (2004) 311.